Pathology - Research and Practice 215 (2019) 215–221

Contents lists available at ScienceDirect

Pathology - Research and Practice

journal homepage: www.elsevier.com/locate/prp

Case report

Ultrastructural immunolocalization of telomerase and hyaluronate in migrating keratinocytes in a case of oro-pharyngeal squamous cancer

Lorenzo Alibardi*

Comparative Histolab Padova and Department of Biology of University of Bologna, Italy

ARTICLE INFO

Keywords:
Oropharyngeal squamous carcinoma
Immunogold
Telomerase
Hyaluronate
Ultrastructure

ABSTRACT

The ultrastructural immunolocalization of telomerase and hyaluronate has been studied in a case of oropharyngeal squamous carcinoma. Immunofluorescence shows that telomerase immunolabeling is present in the cytoplasm and in nuclei of some keratinocytes during their migration into the underlying connective tissue. The electron microscope shows that the nuclear localization of telomerase mainly occurs in the large nucleoli and in likely Cajal bodies, the sites of assembling and maturation of proteins forming the telomerase complex. Aside ribosomes, the nucleolus has a role in the biosynthesis of this reverse transcriptase during cell proliferation in normal tissues and in tumors. The cytoplasmic labeling for telomerase is frequently associated with an irregular network of keratin bundles but the significance of this observation is unclear. Hyaluronate, detected through ultrastructural immunolocalization of a hyaluronate binding protein, is abundant mostly along the cell membrane of the detaching basal keratinocytes during epithelial mesenchymal transition. A coat of hyaluronate surrounds the free keratinocytes of the squamous epithelium and is present around the connective cells present underneath. The study supports the hypothesis that hyaluronate forms a pathway along which epithelial cells can migrate during epidermal mesenchymal transition and may also shield cancer cells from immune cells.

1. Introduction

Oral squamous cell carcinoma is among the more frequent and deadly forms of cancer affecting the oropharyngeal tract [1,2]. A characteristic marker which expression is up-regulated in many tumors is cytoplasmic and/or nuclear telomerase, which primary roles is to sustain the continuous and uncontrolled cell multiplication of neoplastic cells through the regeneration of telomeric ends of dividing chromosomes [3–5]. Although biochemical and light microscopy studies on telomerase localization in different form of squamous carcinomas are available [4–9], the fine distribution of this enzyme at the ultrastructural level in oropharyngeal squamous carcinoma cells is not known.

In addition to telomerases, it is generally known that the epithelia affected by a tumor transformation, including those of the oropharyngeal tract, express higher amount of hyaluronate in all epithelial layers and in cells that invade the connective stroma, with respect to the normal mucosa [2,10,11]. This has been associated to an epithelial-mesenchymal transition (EMT) that determines the migration of epithelial cells into the underlying connective tissues and later into blood vessels, the latter also expressing high hyaluronate levels during metastasis in different types of cancers [10–13]. It is believed that the intense proliferation of cancer cells is favored by telomerase in a permissive extracellular matrix rich in hyaluronate, which also determines the formation of a rich vascular meshwork that promotes the further expansion of the tumor and likely also metastasis.

Studies so far conducted on cancer tissues have shown the general immunolocalization of telomerase [5,8,9] and hyaluronate [10,13]. However the fine distribution of these antigens that could help to determine their sub-cellular localization involved in their movement is insufficiently known. The present study has tackled the problem of the ultrastructural distribution of these antigens in cancer cells in one case of oropharyngeal squamous cell carcinoma. The study confirms and extends the information on the distribution of telomerase and hyaluronate in this type of cancer, and also provides further morphological indication on the origin of telomerases from the nucleolar compartment of malignant cells.

2. Materials and methods

2.1. Fixation and immunofluorescence for telomerase

The material derived from a consent female patient of 88 old years, with a diagnosis of squamous oral carcinoma, to which a mass of about 0.5 cm was removed by surgery. The tissue was fixed in 4% paraformaldehyde in Tris Buffer pH 7.2, dehydrated in ethanol, and

* Corresponding author.

https://doi.org/10.1016/j.prp.2018.10.039
Received 6 September 2018; Received in revised form 28 October 2018; Accepted 31 October 2018

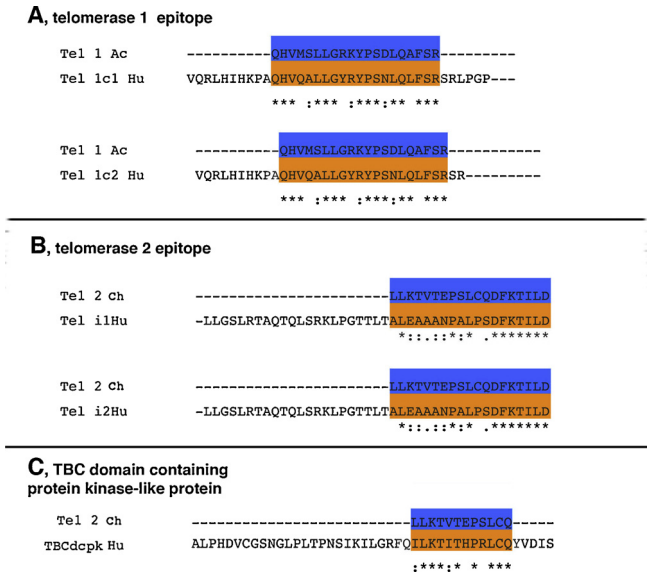

Fig. 1. Bioinformatic analysis reporting the identity between the epitopes of the employed antibodies with those present in the human proteins. **A**, telomerase epitope Tel1 Ac (from *Anolis carolinensis*) recognizes a central region of the human telomerase protein component isoforms 1 (1c1 Hu, NP_001305964.1, aa 454–475) and a human telomerase protein component isoform 2 (1c2 Hu, NP_009041.2, aa 347–368). **B**, the telomerase epitope Te1 2 Ch (from *Gallus gallus*) recognizes a C-terminal region of a human telomerase reverse transcriptase isoform 1 (ilHu, NP_937983.2, aa 115–1132), and the isoform 2 of this protein (i2Hu, NP_001180305.1, aa 1051–1069). **C**, the telomerase epitope (from *Gallus gallus*) also recognizes a human TBC domain-containing protein kinase-like protein isoform a (TBCdcpk Hu, NP_00156907.1 for aa n. 44–54) and also the isoform c of this protein (NP_149106.2, aa 44–55, sequence not shown). Stars represent identities (same amino acid), colons indicate substitutive but conservative replacements (amino acids with similar 3D-shape, size and solubility), dots indicate semi-conserved substitutions (amino acids with similar size but different polarity).

embedded in Lowcryl K4M resin under 2 days of UV light at 0–4 °C. Sections of 2–4 μm were collected with an ultramicrotome on chromo-alume pre-coated slides, and dried on a hot plate for 3–4 h. Sample sections were stained with 1% toluidine blue alkaline solution, for the histological examination. From areas of interest, thin sections were collected at the thickness of 50–90 nm on Copper or Nickel grids of 200 mesh, for the following study under the electron microscope.

For telomerase detection, two rabbit antibodies, previously developed for the study of telomerase in lizard and the chick [14,15], were here utilized for immunolocalization in human tissues (epitopes shown in blue in Fig. 1). These antibodies recognize epitopes with some identity with human telomerase, as determined from the NIH sequence database at https://www.ncbi.nim.nih.gov/pubmed (Fig. 1, orange-colored sequences). For immunofluorescence, some sections were pre-incubated for 30 min at room temperature in a 0.1 M solution of Tris buffer, at pH 7.2, containing 2% of Bovine Serum albumin and 2% Normal Goat Serum, in order to block non-specific antigenic sites. The sections were incubated with the buffer containing the rabbit anti-telomerase 1 or anti-telomerase 2 antibodies at 1: 50 v/v concentration. In control sections, the primary antibody was omitted from the incubating solution. After rinsing with the buffer, a secondary antibody against rabbit, conjugated with FITC (Fluoresceine Isothyocyanate) was applied to the sections of both tests and controls, for one hour at room temperature, at the concentration 1: 100 in buffer. Finally the slides were rinsed in buffer and mounted with Fluoromount, and later observed under a fluorescent microscope equipped with a FITC filter.

2.2. Immunogold for electron microscope detection of telomerase and hyaluronate

For the ultrastructural localization of telomerase present in cancer cells, the two rabbit antibodies indicated above were also utilized on the sections collected on nickel grids. The sections were incubated for 4–5 h at room temperature in the antibody solutions diluted 1:100 in 0.05 M TRIS – HCl buffer at pH 7.6, and containing 1% Cold Water Fish Gelatin. In negative controls, the primary antibody was omitted. After incubation the sections were rinsed in buffer and further incubated for 1 h at room temperature with goat anti-rabbit Gold-conjugated secondary antibody (Sigma, 10 nm gold particles). Grids were rinsed in buffer, dried and stained for 4 min with 2% uranyl acetate, and then observed under the electron microscope (Zeiss C10).

For the detection of hyaluronate, a non-immunogenic biopolymer, an indirect reaction was carried out using the selective binding to hyaluronate from a biotinilated Hyaluronate Binding Protein (HABP) of bovine origin (cat. # 400763, Amsbio, Abingdon, UK). This binding protein was utilized at the concentration of 1: 100 v/v in the incubating solution. The sections on nickel grids were incubated for 6 h at room temperature in 0.05 M Tris – HCl buffer at pH 7.6 containing 1% Cold Water Fish Gelatin. In controls sections, the biotinilated-HABP was omitted in the incubating solution. After the incubation period the sections were rinsed in buffer for three times and incubated for 1 h at room temperature with a goat anti-biotin gold-conjugated antibody (Sigma, 10 nm gold particles) diluted 1: 100 v/v. Some grids went also through a silver enhancing treatment for 5 min to increase the size of gold particles and make the labeling more easily detectable under the electron microscope at low magnification. The suggested intensification method followed the manufacturer instructions (British Biocell International, SEKB250). After the above procedures, the grids were rinsed in the buffer, dried and stained for 4 min with 2% uranyl acetate, rinsed in buffer, distilled water and dried. Both copper and nickel grids were observed under an electron microscope operating at 60 kV (Zeiss C10). Images were recorded either on photographic plates or by a digital camera, and the digitalized images were composed into plates using adobe Photoshop program, version 8.0.

3. Results

3.1. Bioinformatic analysis

The comparison of the epitopes recognized in the lizard (Tel 1) and the human telomerase are shown in Fig. 1A, suggesting that a certain cross-reactivity is likely. Also the other antibody for chicken Telomerase (Tel 2) recognizes in the human protein a stretch of amino acids, also suggesting some cross-reactivity (Fig. 1B). Finally, the Tel 2 antibody recognizes also a shorter epitope present in a protein with kinase activity, indicated as “TBC domain containing protein-kinase like protein” (Fig. 1C, see Discussion), suggesting that the antibody may recognize with less affinity also this short epitope.

3.2. Immunolocalization of telomerase

The histological control showed irregular pegs of epidermal cells migrating inside the connective tissues of the pharyngeal mucosa (Fig. 2A). Keratinocytes possessed large euchromatic nuclei that often contained 2 large nucleoli, and appeared as cells of larger dimension with respect to most cells present in the connective tissue, the stroma (Fig. 2B). Both telomerase 1 and 2 antibodies immunoreacted to the cancer tissues, revealing however sparse immunofluorescent cells with immunofluorescence diffuse in the cytoplasm but also present in some nuclei (Fig. 2C, D). Control sections were immune-negative (Fig. 2E).

The electron microscopy showed the presence of numerous but short bundles of keratin (tonofilaments) in the cytoplasm of squamous keratinocytes forming the compact epithelium (Fig. 3A). Some of these

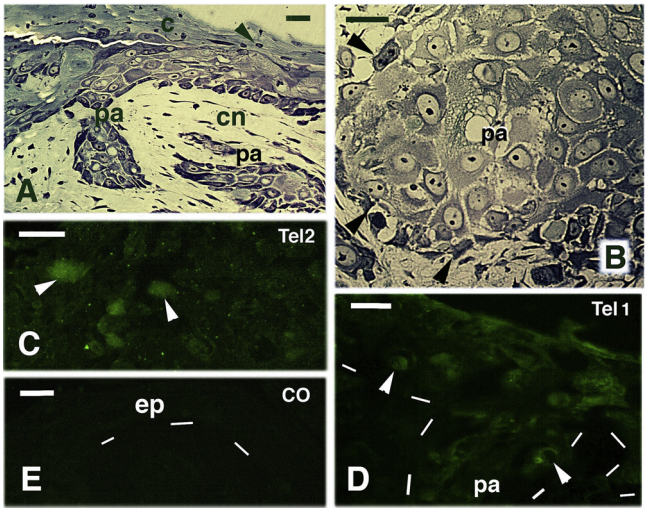

Fig. 2. Histological views (**A, B**) and immunofluorescence images for telomerase 2 (**C-E**) detected in the oral squamous carcinoma. Bars in all figures indicate 10 μm. **A**, area of the altered oral epithelium showing the irregular epithelial papillae (pa) penetrating in the connective tissue (stroma). The arrowhead points to nuclei of corneocytes. (parakeratosis). Toluidine blue stain. **B**, detail on a malignant papilla showing the enlarged keratinocytes featuring euchromatic nuclei and large nucleoli. The external cells (arrowheads) are irregular in shape and their disposition suggests lack of a continuous basement membrane. **C**, telomerase 2 immunolabeling in the epithelium with sparse cells immunopositive (arrowheads). **D**, telomerase 1 immunolabeling in the oral epithelium and papilla (pa, outlined by dashes) showing sparse immunolabeled cells (arrowheads). **E**, immunonegative control section (dashes underline the epithelium, ep) (For interpretation of the references to colour in this figure legend, the reader is referred to the web version of this article).

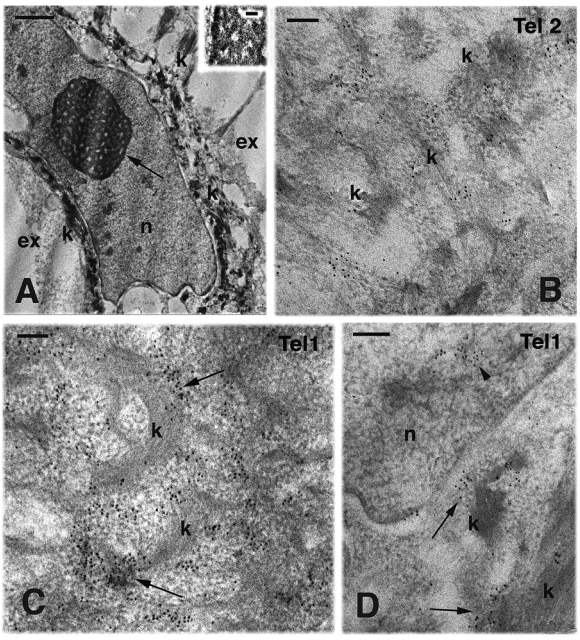

Fig. 3. Electron microscopy details of squamous cells present in the linear epithelium labeled with Tel 1 or Tel 2 antibodies. **A**, general view showing the large nucleus (n) and nucleolus (arrow; enlarged in the inset, Bar, 100 nm), and the cytoplasm tonofilaments (k, keratin). Bar, 1 μm. **B**, cytoplasm labeling among keratin bundles (k). Bar, 100 nm. **C**, detail on the cytoplasmic labeling with clusters associated (arrows) to keratin bundles (k). Bar, 100 nm. **D**, clusters of gold particles near (arrows) bundles of keratin (k) and a cluster (arrowhead) is also noted in the nucleus (n). Bar, 200 nm.

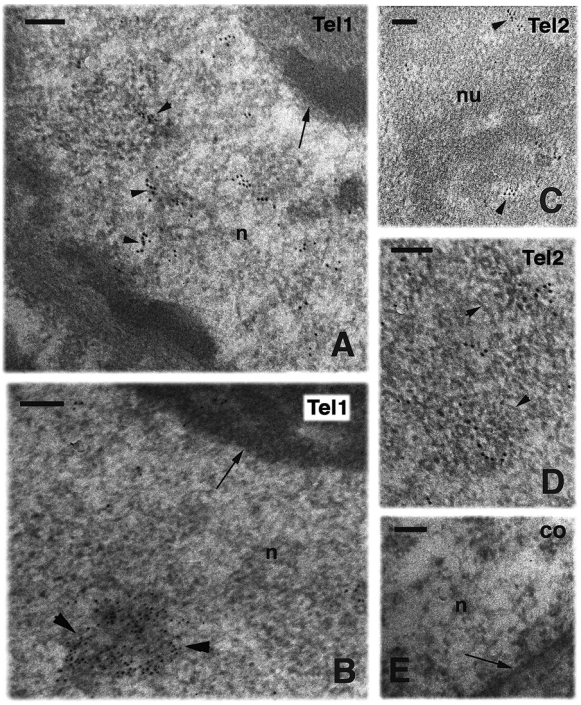

Fig. 4. Ultrastructural labeling in the nucleus of squamous cells with Tel 1 and Tel 2 antibodies. **A**, area of the nucleus (n) showing clusters of gold particles in the nucleoplasm (arrowheads), and near the nucleolus (arrow). Bar, 100 nm. **B**, detail on a denser labeled cluster of gold particles (arrowheads). This likely Cajal body stands out the paler nucleoplasm (n) close to the nucleolus (arrow). Bar, 100 nm. **C**, high magnification detail of the nucleolus (nu), featuring small clusters of gold particles in the paler fibrillar component (arrowheads). Bar, 100 nm **D**, high magnification detail on a likely labeled Cajal body formed by aggregated filaments (arrowheads). Bar, 100 nm. **E**, unlabeled area of the nucleus (n, the arrow indicates the nuclear membrane) present in a control section (CO) of a squamous cell. Bar, 100 nm.

tonofilaments were converging peripherally into the numerous desmosomes present in the central cells of the papillae and linear epithelium (Figs. 2A, 3 A). The large nucleoli see in cancer cells showed a honeycomb meshwork, mainly constituted by the dense fibrous component and sparse granular component, alternated to numerous but small, electron-pale fibrillar centers (inset at higher magnification in Fig. 3A).

Telomerase immunolabeling was present in the cytoplasm of squamous keratinocytes, mainly as clusters of gold particles distributed in the cytoplasm, but these particles were also frequently associated peripherally to keratin bundles or even appeared localized within these bundles (Fig. 3B–D). Also the nuclear labeling was seen in form of cluster of gold particles mainly localized over 10–20 nm thick filaments sparse among the electron-pale nucleoplasm, and likely representing euchromatin (Figs. 3D, 4 A). Denser areas occupied by heterochromatin appeared unlabeled or occasionally labeled. The large nucleolus of squamous keratinocytes was labeled in different areas, but mainly in the fibrillar regions (Fig. 4B, C). Sparse clusters of gold particles were sometimes seen over denser organelles of 0.1–0.3 μm located in the nucleoplasm, containing numerous denser filaments of 10–20 nm in diameter, likely representing Cajal bodies (Figs. 3D, 4 B, D). No diffuse labeling or forming clusters of gold particles was seen in control sections (Fig. 4 E).

3.3. Immunodetection of the HABP for hyaluronate immunolocalization

The immunolabeling showed an intense localization of gold particles of 10 nm in diameter along the surface of keratinocytes of the oral mucosa still associated in an epithelium (Fig. 5 A). Gold particles were

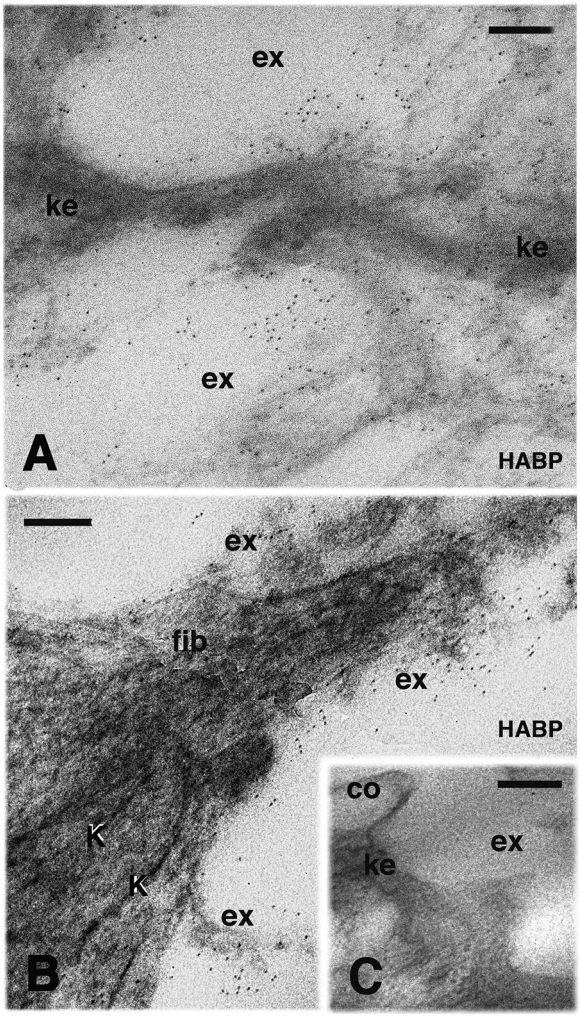

Fig. 5. Ultrastructure of squamous cells that have been immunolabed for HABP (hyaluronate detection) with 10 nm gold particles. **A**, detail on the intense labeling present along the surface and in the extracellular spaces (ex) among squamous keratinocytes elongation. Bar, 200 nm. **B**, other detail on the labeling on the surface and extracellular matrix (ex) of a likely keratinocyte (k indicate keratin bundles) with a fibroblast shape (fib), sparse in the stroma of the cancer tissue. Bar, 200 nm. **C**, detail on unlabeled cytoplasmic elongation of a keratinocyte (ke) and in the extracellular space (ex) of a control section. (CO). Bar, 200 nm.

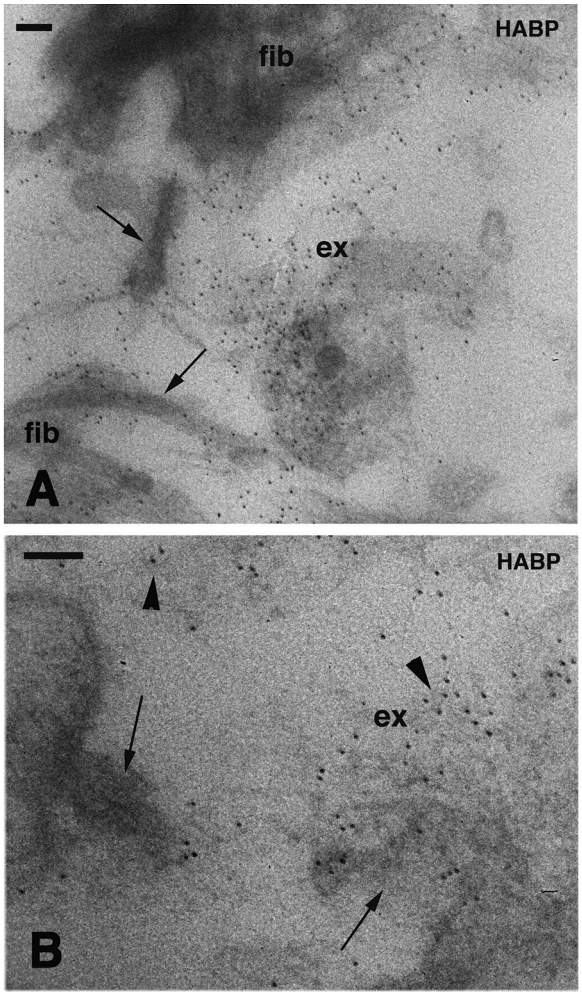

Fig. 6. High magnification details on the HABP immunolabeling in the extracellular spaces of the connective tissue present among the irregular pegs of the squamous epithelium (10 nm gold size). **A**, intense labeling in the amorphous extracellular matrix (ex) surrounding the elongation (arrows) of two fibroblast-like cells (fib) located in the stroma. Bar, 100 nm. **B**, this detail shows that gold particles label the amorphous material (arrows) of the extracellular matrix (ex) and also fine fibrils (arrowheads) likely representing hyaluronate. Bar, 100 nm.

also localized around keratinocytes with a prevalent fibroblastic shape (elongated with rare protrusions), located within the connective tissue found underneath the epithelium (Fig. 5 B). The latter cells were recognized as keratinocytes migrated from the epithelium because of their content in keratin bundles. In control section, no immunolabeling was detected in cells and extracellular matrix (Fig. 5 C). The intense immunolabeling for HABP was extended to the amorphous extracellular matrix surrounding the detached keratinocytes and fibroblasts sparse within the connective tissues (Fig. 6 A). The observation at higher magnification of the amorphous matrix evidenced that the labeling was sometimes associated to fine filaments of about 5–10 nm, likely representing filaments of hyaluronate that also contacted the surface of these cells (Fig. 6 B).

A further confirmation of the distribution of hyaluronate in the cancer tissue was obtained using the silver-intensification methods that showed an intense immunolabeled coating around keratinocytes of the still compacted epithelium (Fig. 7 A), mainly concentrated along the plasma membrane and on the connecting desmosomes among these cells (Fig. 7 B). Finally, the observation on different regions of the irregular epithelial pegs of squamous keratinocytes showed epithelial cells in different stages of a process of EMT. Initially a coat of hyaluronate, detected as an electron-dense precipitate, was present also in the discontinuous basement membrane of the squamous epithelium (Fig. 8 A). Keratinocytes in course of detachment from the epithelium showed an irregular, more or less intense peripheral coat of hyaluronate positive precipitate (Fig. 8 B). A variably dense coat of hyaluronate, as detected though the intense deposition of silver grains, was seen to surround these cells as they detached from the remaining epithelium to assume a mesenchymal and multipolar aspect (Fig. 8 C, D). The free keratinocytes sparse within the connective tissues interspersed among the irregular epithelial pegs (Fig. 2 A) were also coated with a dense precipitate revealing hyaluronate (Fig. 8 D), while their keratin bundles meshwork appeared reduced in comparison to that of keratinocytes still associated in an epithelium.

4. Discussion

4.1. Telomerase distribution in cancer cells

The bioinformatics comparison of the amino acid sequences recognized by the antibodies here utilized (Tel 1 and Tel 2) strongly

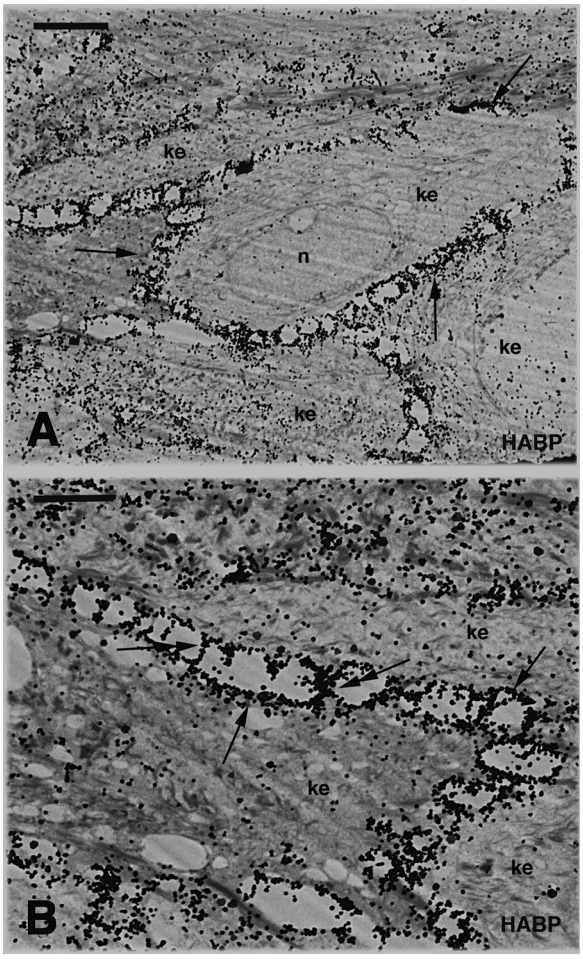

Fig. 7. Immuno-gold and silver intensified sections for HABP detected in squamous cells. **A**, a dense precipitate is observed along the perimeter (arrows) of keratinocytes (ke; n, nucleus). Bar, 5 μm. **B**, a higher magnification view shows that the intense labeling along the cell surface (arrows) extends also to desmosomes (double arrowheads) present among keratinocytes (ke). Bar, 2.5 μm.

indicate that they can immunodetect mainly telomerases also in human tissues (Fig. 1). In general, both antibodies gave a similar immunolocalization at the light and electron microscope level. The principal localization of telomerase was observed in nuclear organelles found in the nucleoplasm, likely representing Cajal bodies, confirming previous observations on cells of regenerating tissues [14,15]. The present study supports the biomolecular data, reporting that these nuclear organelles are involved in the biogenesis and processing of the telomerase complex before it reaches the chromosomes or other cell compartments [16].

The large size and honeycomb pattern of nucleoli observed in cancer cells is correlated to the high rate of ribosome formation and high malignancy of these cells [17–19]. The increase in both fibrillar and granular components seen in the nucleolus of cancer cells appears connected to the decrease in the inhibition of cell proliferation by Retinoblastoma and p53 proteins and conversely by the increased biogenesis of ribosomes [17,19]. In contrast, the reduction in the biogenesis of ribosomes in both normal and cancer cells occurs with the decrease of telomerase expression [18].

The high cytoplasmic labeling associated to keratin filaments observed in squamous cancer cells is a new observation, since it was not evident in cells of the regenerative blastemas in amphibians and lizards [14,15]. The significance of this association of telomerases to keratins in cells of squamous oropharyngeal cancer remains unexplained. However, also light microscopy immunocytochemistry has shown a variable co-localization of keratins and telomerase in the cytoplasm of some tumor cells [20]. A possible function of cytoplasmic telomerase for the reactivation of cell proliferation, metastasis progression, and mitochondrial stress protection remains to be clearly demonstrated [21,22].

4.2. Hyaluronate distribution

The use of a biotinilated binding protein and of an anti-biotin antibody conjugated to gold particles alone or after size enhancing by silver has been previously utilized for the study of the distribution of hyaluronate in embryos [23,24] and in regenerative blastemas of amphibians and lizards [14,15,25,26]. In amphibian blastemas, hyaluronate synthesis has been associated to a stimulating effect largely derived form innervation [27]. Nerves are essential to stimulate blastema formation and initial growth by the release of neurotrophic factors that trigger cell proliferation of mesenchymal and likely also of apical epidermal cells [27–29]. Both blastema cells and regenerating nerves synthesize hyaluronate that is believed to stimulate the growth of nerves and their sheath cells and also of blastema cells [27,29]. Similarly to the blastema, also nerves infiltrating among cells of tumors exert a stimulatory effect on these cells and metastasis, and denervation often stops tumor progression and metastasis, as definitely shown for prostate and gastric cancer [28]. Although the methodology utilized in the present study could not demonstrate the presence of innervation among squamous keratinocytes, it is known that also in oral cancer, malignant cells can spread along nerve fascicles in a process indicated as “perineural invasion” [30].

The present study shows that the production of hyaluronate and its localization in cancer cells resembles that observed for the embryonic tissues and regenerative blastemas, where mesenchymal-like cells of epidermal or true mesenchymal origin migrate following specific pathways and directions. In particular, as epithelial cells detach from the compact epithelium to assume a free, mesenchymal shape during EMT, the coating of hyaluronate remains localized along their cell perimeter, likely favoring their migration into the stroma and possibly metastatic diffusion [11,31,32]. The hyaluronate coating likely allows cell movement but has been also hypothesized that it may form a protective shield against immune cells, allowing mesenchymal cells and cancer cells to resist to the immune attach [31,32].

The ultrastructural localization and distribution of hyaluronate here observed in squamous cancer cells, confirms and specifies the localization previously seen under light microscopy [10,13]. The initial immunohistochemical observations showed that hyaluronate is present in all epithelial layers, including the more external, of squamous cell carcinomas, while the molecule is lower and limited to the basal and suprabasal layers in the normal oral epithelium, and is absent in the simple cylindrical epithelium of the gut and intestine [10]. The prevalent pericellular localization observed in squamous keratinocytes [10] is due to the intense accumulation of hyaluronate along the plasma membrane of these cells (Fig. 7). The lower cytoplasmic labeling for hyaluronate (Fig. 7 B), suggests that the glycosaminoglycan is synthetized intracellularly in both keratinocytes and fibroblasts, but accumulates along the plasma membrane and the irregular basement membrane of the epithelium and of the epithelial papillae (Figs. 2 A, 7 B, 8 A). Furthermore, as the malignant epithelial cells (keratinocytes) move into the underlying connective tissue (stroma), the hyaluronate coat invades also this tissue, and is likely also produced by the stromal cells as squamous keratinocytes penetrate this connective tissue [10,12]. Other studies have shown that the receptor for Hyaluronan Mediated Motility (RHAMM) and Hyaluronan Receptor CD44 are highly expressed in oral squamous cell carcinoma [2,10,13], supporting a fundamental role of hyaluronate in cancer cell migration [11,31,32].

In conclusion, the present ultrastructural study confirms and supports the notion that hyaluronate synthesis and telomerase activation

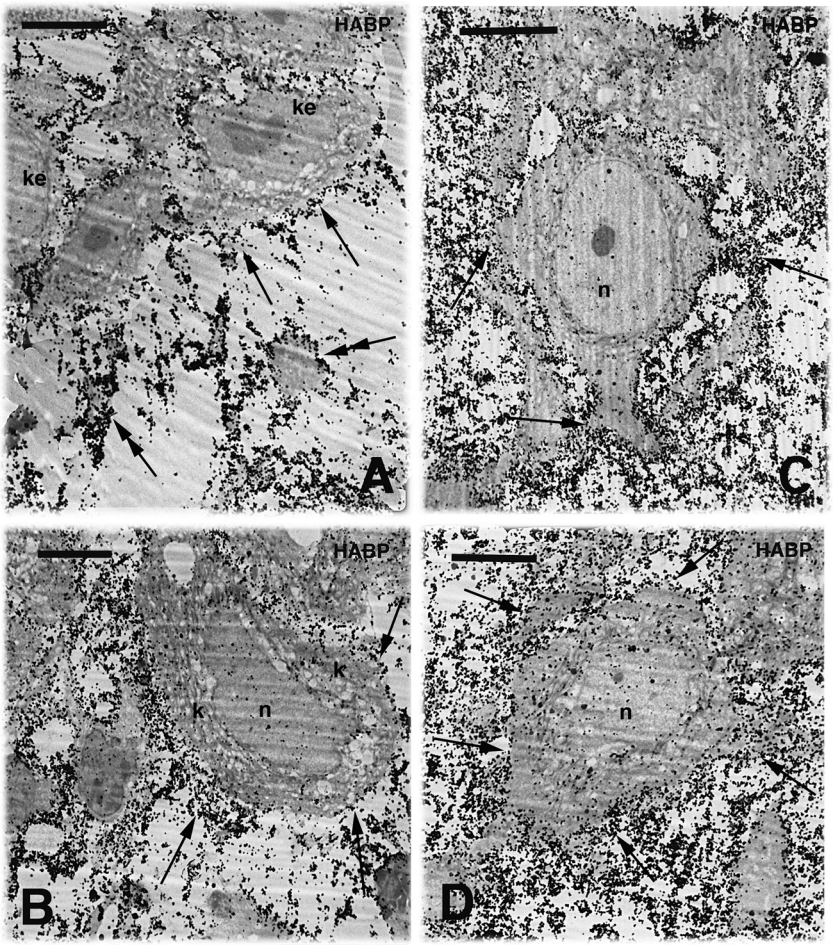

Fig. 8. Immuno-gold and silver intensified sections for HABP in different regions of the squamous epithelium, representing progressive stages of EMT (see text). Scale bars indicate 5 μm in all images. **A**, keratinocytes (ke) still compacted to form an epithelium. The intense labeling (arrows) indicates a discontinuous basement membrane (double arrowheads point to cytoplasmic elongation of keratinocytes within the stromal connective tissue). **B**, image of apparently detaching epithelial cell (n, nucleus) with numerous keratin bundles (k), still surrounded by a coat of hyaluronate labeling (arrows). **C**, other detaching keratinocyte (n, nucleus) featuring an irregular multipolar shape and sparse keratin bundles, and surrounded by a dense hyaluronate precipitate (arrows). **D**, a free keratinocyte (n, nucleus) present within the labeled stroma that shows an intense pericellular labeling (arrows).

are correlated in favoring the growth, expansion and likely metastasis of the tumor. The role of innervation in this process remains to be elucidated using specific microscopic methods.

Acknowledgments

study self-supported, including the TEM analysis. The HABP has been generously donated from Dr. Carla Stecco (Department of Human Anatomy, University of Padova, Italy). The present MS is dedicated to my beloved mother, Pagnin Fides.

References

[1] P.A. Jakobsson, C.M. Eneroth, D. Killander, G. Moberger, B. Martensson, Histological classification and grading of malignancy in carcinoma of the larynx, Acta Radiol. 12 (1973) 1–8.
[2] Y. Yamano, K.M. Uzawa, K. Shinozuka, K. Fushimi, T.H. Ishigami, H. Nomura, K. Ogawara, M. Shiiba, H. Yokoe, H. Tanzawa, Hyaluronan-mediated motility: a target in oral squamous cell carcinoma, Intern. J. Oncol. 32 (2008) 1001–1009.
[3] M. Mayerson, Role of telomerase in normal cancer cells, J. Clin. Oncol. 18 (2000) 2626–2634.
[4] P. Boscolo-Rizzo, M.C. Da Mosto, E. Rampazzo, S. Giunco, A. Del Mistro, A. Menegaldo, L. Baboci, M. Mantovani, C. Tirelli, A. De Rossi, Telomeres and telomerases in head and neck squamous cell carcinoma: from pathogenesis to clinical implications, Canc. Metast. Rev. 35 (2016) (2016) 457–474.
[5] J.W. Shay, Roles of telomeres and telomerase in aging and cancer, Cancer Discov. 6 (2016) 584–593.
[6] S. Hohaus, S. Cavallo, A. Bellacosa, M. Genuardi, J. Galli, G. Cadoni, G. Almadori, L. Lauriola, S. Litwin, M. Maurizi, G. Neri, Telomerase activity in human laryngeal squamous cell carcinomas, Clin. Cancer Res. 2 (1996) 1895–1900.
[7] S.R. Taylor, R.D. Ramirez, M. Ogoshi, M. Chaffin, M.A. Piatyszek, J.W. Shay, Detection of telomerase activity in malignant and normalignant skin conditions, J. Investig. Dermatol. Symp. Proc. 106 (1996) 759–765.
[8] M. Frost, J.B. Bobak, R. Gianani, N. Kin, S. Weinrich, D.C. Spalding, L.G. Cass, L.C. Thompson, T. Enomoto, D. Uribe-Lopez, K.R. Shroyer, Localization of telomerase hTERT protein and hTR in benign mucosa, dysplasia, and squamous cell carcinoma, Am. J. Clin. Pathol. 114 (2000) 726–734.
[9] S. Kyo, K. Masutomi, Y. Maida, T. Kanaya, N. Yatabe, M. Nakamura, M. Tanaka, M. Takarada, I. Sugawara, S. Murakami, T. Taira, M. Inou, Significance of immunological detection of human telomerase reverse transcriptase, Diagn. Mol. Pathol. 163 (2003) 859–867.
[10] C. Wang, M. Tammi, H. Guo, R. Tammi, Hyaluronan distribution in the normal epithelium of esophagus, stomach, and colon and their cancers, Diagn. Mol. Pathol. 148 (1996) 1861–1869.
[11] N. Itano, T. Sawai, O. Miyaishi, K. Kimata, Relationship between hyaluronan production and metastatic potential of mouse mammary carcinoma cells, Cancer Res. 59 (1999) 2499–2504.
[12] B.P. Toole, V.C. Hascall, Commentary. Hyaluronan and tumor growth, Am. J. Pathol. 161 (2002) 745–747.
[13] M.P. Rangel, V.K. de Sa, V. Martins, J.R.M. Martins, E.R. Parra, A. Mendes, P.C. Andrade, R.M. Reis, A. Longatto-Filho, C.Z. Oliveira, T. Takagaki, D.M. Carraro, H.B. Nadr, V.L. Capelozzi, Tissue hyaluronan expression, as reflected in the sputum of lung cancer patients, is an indicator of malignancy, Brasil. J. Med. Biol. Res. 48 (2015) 557–567.
[14] L. Alibardi, Immunolocalization of the telomerase-1 component in cells of the regenerating tail, testis, and intestine of lizards, J. Morphol. 276 (2015) 748–758.
[15] L. Alibardi, Immunodetection of telomerase and PCNA-positive cells in embryonic and juvenile feather follicle of the chick identifies proliferating cells for feather regeneration, Anat. Sci. Internat. (2018).
[16] G.E. Morris, The cajal body, Biochem. Biophys. Acta 1783 (2008) 2108–2115.
[17] L. Montanaro, D. Trere', M. Derenzini, Review. nucleolus, ribosomes and cancer, Diagn. Mol. Pathol. 173 (2008) 301–310.
[18] O. Garcia Gonzalez, R. Assfalg, S. Koch, A. Schelling, J.K. Meena, J. Kraus, A. Lechel, S.F. Katz, V. Benes, K. Scharffetter-Kochanek, H.A. Kestler, C. Gunes, S. Iben, Telomerase stimulates ribosomal DNA transcription under hyperproliferative conditions, Nat. Commun. 5 (2014) 4599.
[19] M. Derenzini, L. Montanaro, D. Trere', Ribosome biogenesis and cancer, Acta Histochem. 119 (2017) 190–197.
[20] N. Zhang, R. Zhang, K. Zou, W. Yu, W. Guo, Y. Gao, J. Li, M. Li, Y. Tai, W. Huang, C. Song, W. Deng, X. Cui, Keratin 23 promotes telomerase reverse transcriptase expression and human colorectal cancer growth, Cell Death Diseases 8 (2017) e2961.
[21] J. Mavrommatis, E. Mylona, H. Gakiopoulou, C. Stravodimos, A. Zervas, A. Giannopulos, L. Nakopoulou, Nuclear hTERT immunohistochemical expression is

associated with survival of patients with urothelial bladder cancer, Anticancer Res. 25 (2005) 3109–3116.
[22] I. Chiodi, C. Mondello, Telomere-independent functions of telomerase in nuclei, cytoplasm, and mitochondria, Front. Oncol. 2 (2012) 133.
[23] J.M. Estes, N.S. Adzick, M.R. Harrison, M.T. Longaker, R. Stern, Hyaluronate metabolism undergoes an ontogenic transition during fetal development: implications for scar-free wound healing, J. Pediat. Surg. 28 (1993) 1227–1231.
[24] E.G. Contreras, M. Gaete, N. Sanchez, H. Carrasco, J. Larrain, Early requirement of hyaluronan for tail regeneration in *Xenopus* tadpoles, Development 136 (2009) 2987–2996.
[25] B.P. Toole, Hyaluronan in morphogenesis, J. Inter. Med. 242 (1997) 35–40.
[26] L. Alibardi, Ultrastructural immunolocalization of hyaluronate in regenerating tail of lizards and amphibians supports an immune-suppressive role to favor regeneration, J. Morphol. 279 (2017) 176–186.
[27] A.L. Mescher, C.A. Cox, Hyaluronate accumulation and nerve-dependent growth during regeneration of larval *Ambystoma* limbs, Differentiation 38 (1988) 161–168.
[28] B. Boilly, S. Faulkner, P. Jobling, H. Hondermarck, Nerve dependence: from regeneration to cancer, Cancer Cell 31 (2017) 342–354.
[29] H.E. Young, B.K. Dalley, R.R. Markwald, Identification of hyaluronate within peripheral neural tissue matrices during limb regeneration. Developing and regenerating vertebrate nervous systems, Alan Liss Inc., New York, 1983, pp. 175–183 10011.
[30] N.O. Binmadi, J.R. Basile, Perineural invasion in oral squamous cell carcinoma: a discussion of significance and review of the literature, Oral Oncol. 47 (2011) 1005–1010.
[31] H.H. Epperlein, N. Radomski, F. Wonka, P. Walther, M. Wilsch, M. Muller, H. Schwarz, Immunohistochemical demonstration of hyaluronan and its possible involvement in axolotl neural crest migra- tion, J. Struct. Biol. 132 (2000) 19–32.
[32] A.B. Csoka, R. Stern, Hypotheses on the evolution of hyaluronan: a highly ironic acid, Glycobiology 23 (2013) 398–411.